ISSN 0021-3640, JETP Letters, 2014, Vol. 100, No. 6, pp. 376–379. © Pleiades Publishing, Inc., 2014.
Original Russian Text © B.B. Straumal, A.R. Kilmametov, Yu.O. Kucheev, K.I. Kolesnikova, A. Korneva, P. Zięba, B. Baretzky, 2014, published in Pis'ma v Zhurnal Eksperimental'noi i Teoreticheskoi Fiziki, 2014, Vol. 100, No. 6, pp. 418–422.

Transformation of Hume-Rothery Phases under the Action of High Pressure Torsion

B. B. Straumal[a–d], A. R. Kilmametov[d], Yu. O. Kucheev[a, b, d], K. I. Kolesnikova[a, b], A. Korneva[e], P. Zięba[e], and B. Baretzky[d]

[a] *Institute of Solid State Physics, Russian Academy of Sciences, Chernogolovka, Moscow region, 142432 Russia*
e-mail: straumal@issp.ac.ru
[b] *National University of Science and Technology MISIS, Leninskii pr. 4, Moscow, 119049 Russia*
[c] *Moscow Institute of Physics and Technology (State University), Institutskii per. 9, Dolgoprudnyi, Moscow region, 141700 Russia*
[d] *Institut für Nanotechnologie, Karlsruher Institut für Technologie, Hermann-von-Helmholtz-Platz 1, 76344 Eggenstein-Leopoldshafen, Germany*
[e] *Instytut Matalurgii i Inżynierii Materiałowej, ul. W. Reymonta 25, 30-059 Kraków, Poland*

Received July 25, 2014

It has been revealed experimentally that high-pressure torsion induces phase transformations of certain Hume-Rothery phases (electron compounds) to others. High-pressure torsion induces the $\zeta \longrightarrow \delta + \varepsilon$ reaction in copper–tin alloys with the appearance of the $\delta + \varepsilon$ phase mixture as after long-term annealing in the temperature range $T_{\text{eff}} = 350–589$°C. The mass transfer rate driven by high-pressure torsion is 14–18 orders of magnitude higher than the rate of conventional thermal diffusion at the processing temperature T_{HPT}. This phenomenon can be explained by an increased concentration of defects (in particular, vacancies) in the steady state under high-pressure torsion, which is equivalent to an increase in the temperature.

DOI: 10.1134/S0021364014180106

Severe plastic deformation can induce various phase transformations in solids [1–4]. In other words, the composition and structure of phases in a sample after severe plastic deformation can differ from those before deformation. In particular, the decomposition of supersaturated solid solutions [2, 5–7], the saturation of the matrix with the second component (formation of solid solutions) [6, 7], the formation of one or two different amorphous phases from crystalline phases [8–10], the decomposition of an amorphous phase with the formation of nanocrystals [11, 12], and allotropic phase transformations (e.g., α–ε Co, α–γ Fe, α–β–ω Ti, or α–β–ω Zr) [2, 4, 13–16] can occur. However, all listed phenomena were observed in phases with a relatively simple crystal lattice such as an fcc lattice with the space group *Fm*3*m*, a bcc lattice with the space group *Im*3*m*, and an hcp lattice with the space group *P*63. It would be interesting to study severe plastic-deformation-induced evolution of phases in which a small change in the concentration can result in a strong change in a crystal lattice with a large unit cell. A good object for such study is a copper–tin system, where the so-called Hume-Rothery phases (or electron compounds) are formed. Hume-Rothery phases appear in a certain sequence when atoms with valence from two to five (tin, zinc, indium, etc.) are added to a matrix composed of single-valence atoms (copper, silver, or gold) [17, 18].

An alloy of copper with 36 wt % tin (copper with a purity of 99.998 wt % and tin with a purity of 99.999 wt %) was manufactured by inductive melting in vacuum. The resulting ingots with a diameter of 10 mm were cut by means of spark erosion into 0.7-mm-thick disks. Some of these disks were sealed into quartz ampoules with a residual pressure of 4×10^{-4} Pa for subsequent annealing. Other disks were subjected to high-pressure torsion in a Bridgman anvil chamber (W. Klement GmbH, Lang, Austria) at a pressure of 7 GPa, five revolutions with a speed of 1 rpm at room temperature. In this regime, a steady state of the sample is already reached after one and a half revolutions of anvils. In the process of subsequent deformation, torque for high-pressure torsion does not change. The samples for subsequent structure studies were cut at a distance of 3 mm from the center of the deformed disk. The ampoules with the samples were annealed in a SUOL resistance furnace at temperatures of 320°C (1200 h), 500°C (894 h), and 600°C (530 h). The points corresponding to annealing temperatures and concentrations of the alloy with 36 wt % tin are shown by open circles on the phase diagram of Cu–Sn in Fig. 1. They lie in the two-phase regions (Cu) + ε, (Cu) + δ, and (Cu) + ζ, respectively. After annealing, the samples were quenched in water (ampoules were broken). A cast sample before and after high-pressure torsion was mechanically ground

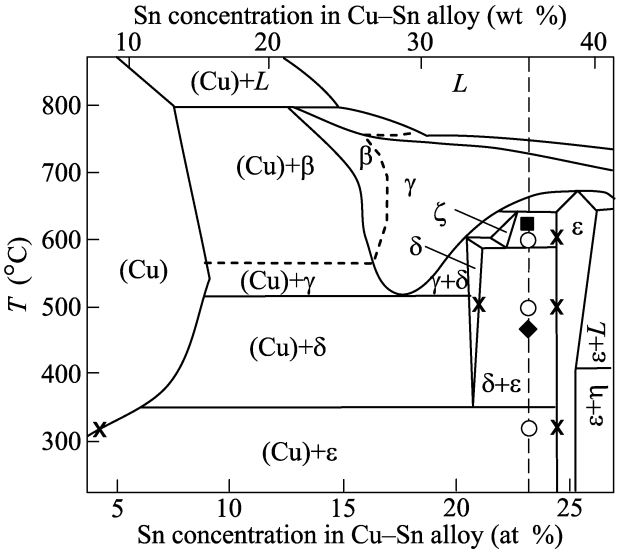

Fig. 1. Part of the phase diagram of Cu–Sn [19]. The thick solid and thick dashed lines correspond to first- and second-order phase transitions, respectively. The vertical dashed line indicates the alloy under study. Open circles mark the temperatures of long-term annealing. Crosses correspond to the phase compositions. The closed square and closed diamond indicate the phase compositions of the cast alloy before and after high-pressure torsion, respectively.

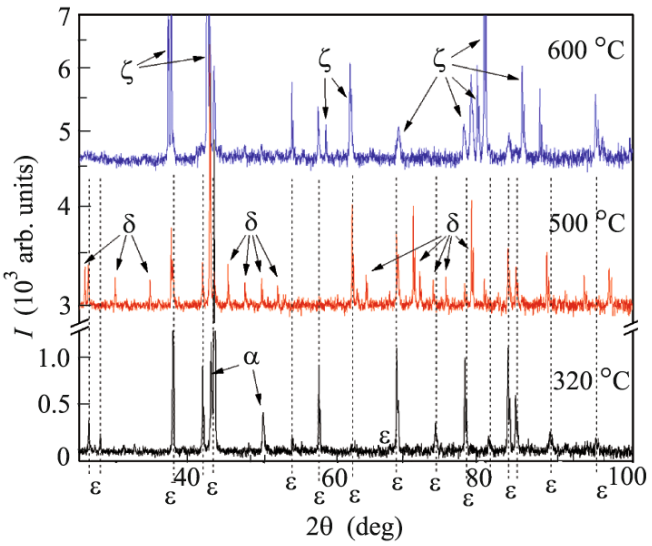

Fig. 2. (Color online) X-ray diffraction patterns of the Cu–36 wt % Sn alloy after long-term annealing at temperatures of 320, 500, and 600°C.

and polished with a diamond paste with a granularity of 1 μm. The resulting slice was examined by optical microscopy with a Neophot-32 microscope equipped with a 10 Mpix Canon Digital Rebel XT camera, as well as by scanning electron microscopy and X-ray microanalysis with a Philips XL30 scanning electron microscope equipped with a LINK ISIS energy dispersion spectrometer (Oxford Instruments). X-ray diffraction patterns were obtained in the Bragg–Brentano geometry on a Philips X'Pert powder diffractometer with the use of Cu-$K\alpha$ radiation. The lattice parameter was determined by means of the Fityk program [20]. The phases in alloys were identified by comparing with the X'Pert HighScore Panalytical phase database [21].

Figure 2 shows the X-ray diffraction patterns of the annealed samples. Greek letters mark the peaks of the corresponding crystal phases. It can be clearly seen that quenching after annealing really allows conserving crystal phases existing in the process of annealing according to the equilibrium phase diagram (Fig. 1). In particular, the α and ε phases are observed in the sample after annealing at 320°C. The α phase (or (Cu)) is a copper-based solid solution with the fcc structure, the space group $Fm3m$, and the lattice constant $a = 0.365233$ nm. This constant is somewhat larger than that in pure copper (0.362 nm [7]) because of tin dissolved in the (Cu) phase. The ε phase (or Cu_3Sn) has an orthorhombic structure with the space group $Cmcm$ [22] and lattice constants $a = 0.55095$ nm, $b = 3.81629$ nm, and $c = 0.43276$ nm. A mixture of the δ and ε phases is observed in the sample after annealing at a temperature of 500°C. The δ phase (or $Cu_{41}Sn_{11}$) has a cubic structure with the space group $F\bar{4}3m$ [23] and the lattice constant $a = 1.79632$ nm. The ζ and ε phases are observed in the sample after annealing at a temperature of 600°C. The ζ phase (or $Cu_{10}Sn_3$) has a hexagonal structure with the space group $P63$ [24] and the lattice constants $a = b = 0.73294$ nm and $c = 0.78685$ nm. The ε, δ, and ζ phases have narrow homogeneity regions on the phase diagram of Cu–Sn (Fig. 1) and are daltonides.

The X-ray patterns of phases that can be observed in cast samples and samples after high-pressure torsion were obtained in the experiments. Comparison with the patterns of annealed and quenched samples simplified the identification of the crystal structure of the samples after high-pressure torsion, because all indicated samples have quite complex crystal structures and large unit cells. Figure 3 shows X-ray diffraction patterns of the cast sample before and after high-pressure torsion. The cast sample contains the ζ and ε phases similar to the sample after annealing at 600°C. These phases appear in the process of solidification and subsequent cooling of the ingot. The composition of the cast sample is shown in the phase diagram of Cu–Sn (Fig. 1) by a closed circle in the ζ + ε two-phase region. This means that subsequent phase transformations (in particular, the eutectoid decomposition of the ζ phase into a mixture of the δ and ε phases at 589°C) were kinetically suppressed at cooling of the solidified ingot below a temperature of 589°C. The diffraction peaks in the cast sample are slightly broadened as compared to the sample after annealing at

600°C owing to the separation (because different regions of the sample under solidification acquire different compositions approximately in the interval from 32 to 40 wt % Sn, see the phase diagram in Fig. 1), and small peaks are joined with each other. The lattice constants in the ε phase of the cast alloy are $a = 0.55124$ nm, $b = 3.82427$ nm, and $c = 0.43372$ nm. The lattice constants in the ζ phase of the cast alloy are $a = b = 0.73324$ nm and $c = 0.78744$ nm. The grain size in the cast sample determined by means of scanning electron microscopy is 50–200 μm.

Peaks in the X-ray diffraction spectrum of the cast sample after high-pressure torsion are wider. This indicates the strong grain refinement in the alloy, which is usual for high-pressure torsion, and the appearance of significant microdistortions of the crystal lattice in the deformed material. Since the symmetry of the crystal lattice of the ε, δ, and ζ phases is low, the modified Williamson–Hall method cannot be used to correctly determine the crystallite size and microstresses after high-pressure torsion in terms of the broadening of X-ray diffraction peaks [25]. The qualitative estimate of the width of the lines and comparison with previous works on the high-pressure torsion of copper alloys [2, 4, 6, 7] implies that the grain size after high-pressure torsion does not exceed 200–300 nm. The cast alloy after high-pressure torsion consists of a mixture of the δ and ε phases. The ζ phase, present in the cast sample, is not observed. Consequently, the ζ phase is decomposed in the process of deformation into the mixture of the δ and ε phases. The lattice constants in the ε phase are $a = 0.55118$ nm, $b = 3.8338$ nm, and $c = 0.43415$ nm. The lattice constant in the δ phase is $a = 1.80395$ nm. Thus, the lattice constants of the ε, δ, and ζ phases in the cast sample before and after high-pressure torsion hardly differ from the table values and our values measured in the samples after long-term annealing. In particular, this means that the decomposition of the ζ phase at high-pressure torsion is accompanied by the formation of the δ and ε phases of another composition (Fig. 1) and by the deformation-induced mass transfer similar to diffusion.

We compare deformation-stimulated mass transfer and conventional thermal diffusion. The bulk diffusion coefficient D_{HPT} necessary for such mass transfer can formally be estimated by the formula $L = (D_{HPT}t)^{0.5}$. The duration t of the high-pressure torsion process is 300 s. The distance L at which mass transfer occurs can be estimated as half of the dimension of grains after high-pressure torsion, i.e., $L \sim 100$ nm. Correspondingly, $D_{HPT} \sim 10^{-17}$ m^2/s. The extrapolation of D for bulk self-diffusion in copper to 300 K (temperature of high-pressure torsion T_{HPT}) and bulk diffusion of tin in copper gives $D = 10^{-35}$ m^2/s [26] and $D = 10^{-31}$ m^2/s [27], respectively. Although the pressure reduces the bulk and grain-boundary diffusion coefficients [28, 29], D_{HPT} is 14–18 orders of magnitude larger than these extrapolated values. This means that high-pressure torsion strongly accelerates mass transfer as in our preceding experiments.

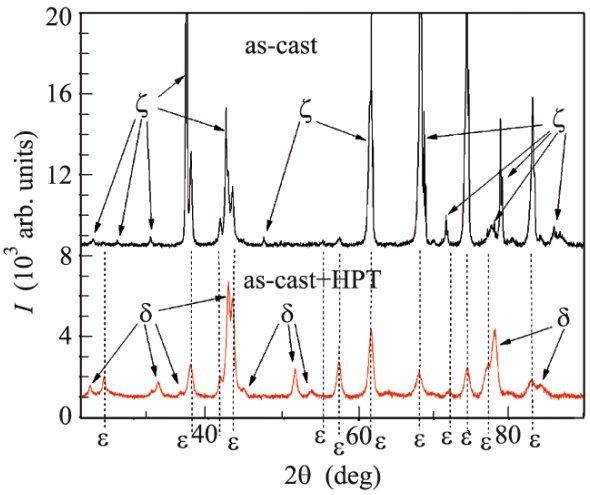

Fig. 3. (Color online) X-ray diffraction patterns of the Cu–36 wt % Sn cast alloy before and after high-pressure torsion.

The phase composition of the high-pressure torsion alloy appears the same as in the sample after annealing at 600°C (i.e., δ + ε). It is shown in the phase diagram of Cu–Sn (Fig. 1) in the δ + ε two-phase region by the closed diamond. The temperature T_{eff} at which phases appearing at the severe external action on the system can be found in the equilibrium phase diagram is called the efficient temperature [30]. In our case, it can be determined quite accurately because the region of the coexistence of the δ + ε phases in the phase diagram of Cu–Sn is fairly narrow, $T_{eff} = 350$–589°C [19]. If the ζ phase were decomposed into the α + ε mixture, T_{eff} would be below 350°C, whereas the temperature T_{eff} in the case of the transformation of the ζ + ε mixture to the γ phase would be above 670°C. We previously determined T_{eff} from the solubility of the second component in the matrix after high-pressure torsion [2, 6, 7], from the presence of low-temperature allotropic modifications [2], or from the presence of an amorphous phase (analog of the melt in the phase diagram [30]) after high-pressure torsion [4, 10]. If the diffusion coefficient is extrapolated to T_{eff} rather than to the high-pressure torsion temperature $T_{HPT} = 300$ K, the coefficients obtained for the bulk self-diffusion in copper and bulk diffusion of tin in copper are $D = 10^{-17}$ m^2/s and $D = 10^{-15}$ m^2/s [27], respectively, which almost coincide with D_{HPT}. This phenomenon can be explained by an increased concentration of defects (in particular, vacancies) in the steady state under high-pressure torsion, which is equivalent to an increase in the temperature.

In summary, we have found for the first time that high-pressure torsion induces phase transformations of certain Hume-Rothery phases (electron compounds) to others. High-pressure torsion is accompanied by the appearance of the $\delta + \varepsilon$ phase mixture in copper–tin alloys as after long-term annealing in the temperature range $T_{\text{eff}} = 350$–589°C. The observed $\zeta \longrightarrow \delta + \varepsilon$ transformation requires mass transfer. The rate of this mass transfer is 14–18 orders of magnitude higher than the rate of conventional thermal diffusion at the processing temperature T_{HPT}, but is close to the diffusion rate at T_{eff}. This phenomenon can be explained by an increased concentration of defects (in particular, vacancies) in the steady state under high-pressure torsion, which is equivalent to an increase in the temperature.

This work was supported by the Russian Foundation for Basic Research (project no. 14-08-00972), by the National Science Centre of Poland (grant nos. DEC-2011/01/M/ST8/07822 and OPUS 254045), and in part by the National University of Science and Technology MISIS (research project K2-2014-013).

REFERENCES

1. X. Sauvage, A. Chbihi, and X. Quelennec, J. Phys.: Conf. Ser. **240**, 012003 (2010).
2. B. B. Straumal, A. A. Mazilkin, B. Baretzky, E. Rabkin, and R. Z. Valiev, Mater. Trans. **53**, 63 (2012).
3. S. K. Pabi, J. Joardar, and B. S. Murty, Proc. Ind. Nac. Sci. Ac. A **67**, 1 (2001).
4. B. Straumal, A. Korneva, and P. Zięba, Arch. Civil Mech. Eng. **14**, 242 (2014).
5. B. B. Straumal, B. Baretzky, A. A. Mazilkin, F. Phillipp, O. A. Kogtenkova, M. N. Volkov, and R. Z. Valiev, Acta Mater. **52**, 4469 (2004).
6. B. B. Straumal, S. G. Protasova, A. A. Mazilkin, E. Rabkin, D. Goll, G. Schütz, B. Baretzky, and R. Valiev, J. Mater. Sci. **47**, 360 (2012).
7. B. B. Straumal, A. R. Kilmametov, Yu. O. Kucheev, L. Kurmanaeva, Yu. Ivanisenko, B. Baretzky, A. Korneva, P. Zięba, and D. A. Molodov, Mater. Lett. **118**, 111 (2014).
8. S. D. Prokoshkin, I. Yu. Khmelevskaya, S. V. Dobatkin, I. B. Trubitsyna, E. V. Tatyanin, V. V. Stolyarov, and E. A. Prokofiev, Acta Mater. **53**, 2703 (2005).
9. X. Sauvage, L. Renaud, B. Deconihout, D. Blavette, D. H. Ping, and K. Hono, Acta Mater. **49**, 389 (2001).
10. A. A. Mazilkin, G. E. Abrosimova, S. G. Protasova, B. B. Straumal, G. Schütz, S. V. Dobatkin, and A. S. Bakai, J. Mater. Sci. **46**, 4336 (2011).
11. A. M. Glezer, M. R. Plotnikova, A. V. Shalimova, and S. V. Dobatkin, Bull. Russ. Ac. Sci. Phys. **73**, 1233 (2009).
12. S. Hóbor, Á. Révész, A. P. Zhilyaev, and Zs. Kovács, Rev. Adv. Mater. Sci. **18**, 590 (2008).
13. Y. Ivanisenko, I. MacLaren, X. Sauvage, R. Z. Valiev, and H.-J. Fecht, Acta Mater. **54**, 1659 (2006).
14. M. T. Pérez-Prado and A. P. Zhilyaev, Phys. Rev. Lett. **102**, 175504 (2009).
15. K. Edalati, E. Matsubara, and Z. Horita, Metal. Mater. Trans. A **40**, 2079 (2009).
16. Y. Ivanisenko, A. Kilmametov, H. Roesner, and R. Z. Valiev, Int. J. Mater. Res. **99**, 36 (2008).
17. V. F. Degtyareva and Yu. A. Skakov, Sov. Phys. Crystallogr. **21**, 222 (1976).
18. Ya. S. Umanskii and Yu. A. Skakov, *Physics of Metals (Atomic Structure of Metals and Alloys)* (Metallurgiya, Moscow, 1978) [in Russian].
19. S. Fürtauer, D. Li, D. Cupid, and H. Flandorfer, Intermetallics **34**, 142 (2013).
20. M. Wojdyr, J. Appl. Crystallogr. **43**, 1126 (2010).
21. D. Smith et al., ICDD Grant-in-Aid (Penn State Univ., Univ. Park, Pennsylvania, 1978).
22. Y. Watanabe, Y. Fujinaga, and H. Iwasaki, Acta Crystallogr. B **39**, 306 (1983).
23. M. H. Booth, J. K. Brandon, R. Y. Brizard, C. Chieh, and W. B. Pearson, Acta Cryst. B **33**, 30 (1977).
24. J. K. Brandon, W. B. Pearson, and D. J. N. Tozer, Acta Crystallogr. B **31**, 774 (1975).
25. J. Markmann, V. Yamakov, and J. Weissmueller, Scripta Mater. **59**, 15 (2008).
26. S. Fujikawa and K. I. Hirano, in *Proceedings of Yamada 5th Conference on Point Defects, Defect Interactions in Metals* (Univ. of Tokyo Press, Tokyo, 1982), p. 554.
27. V. A. Gorbachev, S. M. Klotsman, Ya. A. Rabovskiy, V. K. Talinskiy, and A. N. Timofeyev, Phys. Met. Metallogr. **35**, 226 (1973).
28. B. B. Straumal, L. M. Klinger, and L. S. Shvindlerman, Scripta Metal. **17**, 275 (1983).
29. D. A. Molodov, B. B. Straumal, and L. S. Shvindlerman, Scripta Metal. **18**, 207 (1984).
30. G. Martin and P. Bellon, Solid State Phys. **50**, 189 (1997).

Translated by R. Tyapaev